Probing for Exoplanets Hiding in Dusty Debris Disks: Inner *Disk* *Imaging*, *Characterization*, and *Exploration* with HST/STIS Multi-Roll Coronagraphy

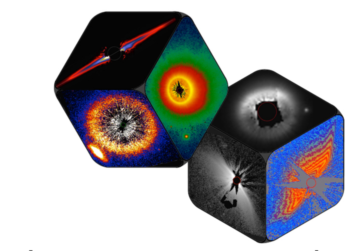

Glenn Schneider (University of Arizona) and the *HST*/GO 12228 Team:

Joseph Carson[1], John Debes[2], Miwa Goto[3], Carol Grady[4], Thomas Henning[3], Dean Hines[2], Phil Hinz[5], Hannah Jang-Condell[6], Mark Kuchner[7], Amaya Moro-Martin[8], Marshall Perrin[2], Gene Serabyn[9], Murray Silverstone[10], Christopher Stark[11], Motohide Tamura[12], Alycia Weinberger[11], John Wisniewski[13], Bruce Woodgate[7]

[1]College of Charleston, [2]STScI, [3]MPIA, [4]Eurkea Scientific, [5]U. Arizona, [6]U. Wyoming, [7]NASA/GSFC, [8]CSIC-INTA, [9]JPL/Caltech, [10]U. Alabama, [11]CIW, [12]NAOJ, [13]U. Washington

ABSTRACT

We present new, preliminary, observational results from the first three of a sample of eleven circumstellar (CS) debris disks, all with HST pedigree and host stars spanning spectral types M1-A0 and a factor of 100 in age, using STIS visible-light PSF-subtracted multi-roll coronagraphic imaging: **HD 181327**, **AU Mic** (both ~ 12 Myr old members of the β Pic moving group) and the order of magnitude older solar analog **HD 107146**. Our ongoing observations from HST/GO program 12228 are probing the interior CS regions of these debris systems, with inner working distances of < appx 8 AU for half the stars in our sample, corresponding to the giant planet and Kuiper belt regions within our own solar system. The new images we are obtaining enable direct inter-comparison of the architectures of exoplanetary debris systems in the context of our own Solar System. These observations also permit us, for the first time, to characterize material in these regions at high spatial resolution and identify disk sub-structures that are signposts of planet formation and evolution; in particular, asymmetries and non-uniform debris structures that signal the presence of co-orbiting perturbing planets. All of our objects were observed previously at longer wavelengths (but much lower spatial resolution and imaging efficacy) with NICMOS, but with an r=0.3" IWA comparable to STIS multi-roll coronagraphy. The combination of new optical and existing near-IR imaging can strongly constrain the dust properties, thus enabling an assessment of grain processing and planetesimal populations. These results will directly inform upon the posited planet formation mechanisms that occur after the ~ 10 My epoch of gas depletion, at a time in our solar system when giant planets were migrating and the terrestrial planets were forming, and directly test theoretical models of these processes. These observations uniquely probe into the interior regions of these systems for the first time with spatial resolution comparable to ACS and with augmenting NICMOS near-IR disk photometry in hand.

THE HST/GO 12228 TARGET SAMPLE

TARGET	Bmag	B-V	Sp.	Distance(pc)	Age(Myr)	HST Initial Imaging	(Reference)
PDS66	11.36	+1.01	K1Ve	~86	13 +/-7	NICMOS	Cortes et al 2009
HD32297	8.33	+0.20	A0V	112.4 ± 10.7	~ 10	NICMOS	Schneider et al 2005
HD15115	7.15	+0.35	F2	45.2 ± 1.3	12 (?)	ACS	Kalas et al 2007a
HD181327*	**7.51**	**+0.48**	**F6V**	**51.8 ± 1.7**	**12 — 20**	**NICMOS/ACS**	**Schneider et al 2006**
AU MIC*	**10.05**	**+1.44**	**M1Ve**	**9.91 ± 0.10**	**12 (+8,-4)**	**ACS†**	**Krist et al 2005**
HD61005	8.93	+0.71	G8V	34.4 ± 1.1	90 +/-40	NICMOS	Hines et al 2006
HD107146*	**7.69**	**+0.62**	**G2V**	**27.5 ± 0.41**	**80 — 200**	**ACS**	**Ardila et al 2004/05**
HD92945	8.65	+0.89	K1V	21.4 ± 0.3	80 — 300	ACS	Golimowski et al 2011
HD15745	7.82	+0.32	F2V	63.5 ± 2.4	~100 (?)	ACS	Kalas et al 2007b
HD139664	5.04	+0.40	F2V	17.52 ± 0.22	300 (+700, -200)	ACS	Kalas et al 2006
HD53143	7.61	+0.80	G9V	18.33 ± 0.11	1000 +/-300	ACS	Kalas et al 2006

**1st GO/12228 results reported herein.*

†AU MIC: ground-based discovery imaging: Kalas et al 2004.

SUMMARY OF OBSERVATIONAL DISK CHARACTERISTICS (Stay Tuned, MORE to Come!...)

STAR	Morphology	Inner Clearing?	Outermost Extent	Brightness Asymmetries	Stellocentric Offset?	0.6 μm Disk Flux Density	f_*/f_{disk} (0.6 μm)
HD 181327	Inclined Narrow Ring + Diffuse Outer Halo	Yes. Sharp Inner Edge @ 25 – 30 AU	~ 460 AU (asymmetric)	Yes. Non H-G azimuthal. Inner/outer skew. 25% ansal SB difference	Yes	7.81 mJy	0.17% ± 0.015%
AU MIC	Edge-On	---	~ 130 AU (symmetric)	Yes. Out-of-plane. Warp. Sub-structures.	N/A	2.51 mJy	0.20% ± ~ 0.02%
HD 107146	Near Face-On Broad Ring	Yes. Shallow Inner Edge @ ~ 60 AU	~ 220 AU (symmetric)	Yes. (H-G scattering phase angle only)	TBD	0.404 mJy	0.0077% ± ~ 0.0004%

HD 181327

Our new six-roll combined PSF-template subtracted STIS coronagraphic imaging of the HD 181327 debris disk (Fig 1A) reveals previously unseen sub-structures and asymmetries that may implicate the presence of yet unimaged planetary-mass perturbers. The bright narrow ring of starlight-scattering material (Fig 1B), brightest at r = 1.86" (88.5 AU projected distance), exhibits non-axisymmetric surface brightness (SB) asymmetries (Fig 1C) that cannot be explained by simple directionally scattering preferential (e.g., Henyey & Greenstein [H-G] 1941) by the disk grains.

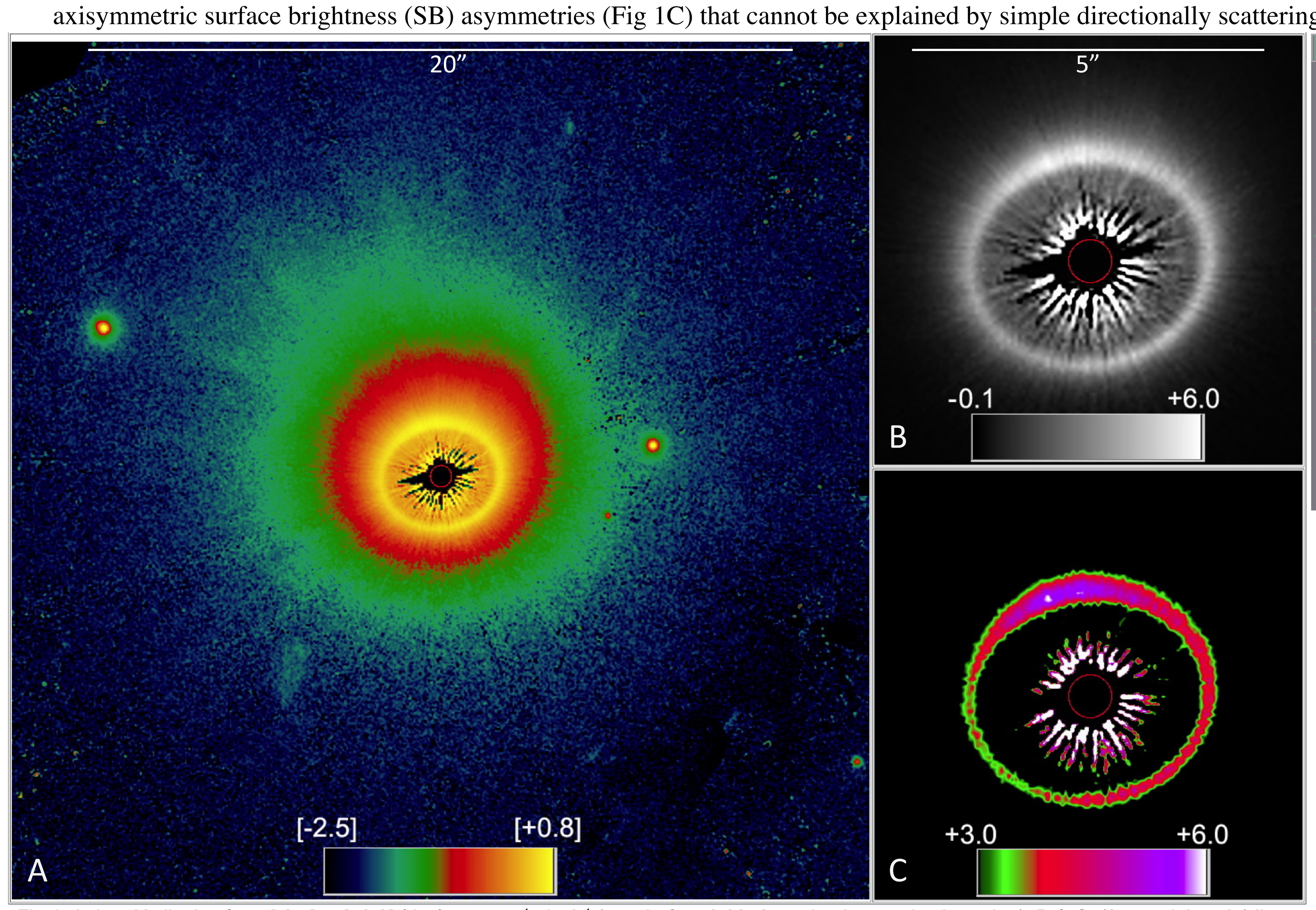

Fig 1. A: Log10 display from [-2.5] to [+0.8] {dex} count s⁻¹ pixel⁻¹ (csp; before 0.0056 csp background subtraction). B & C: (2x spatial scale) linear displays to illustrate the narrow width and "sharpness" of the bright ring and SB asymmetries. 1 csp = 177 microJy arcsec⁻². Red circle: r = 0.3".

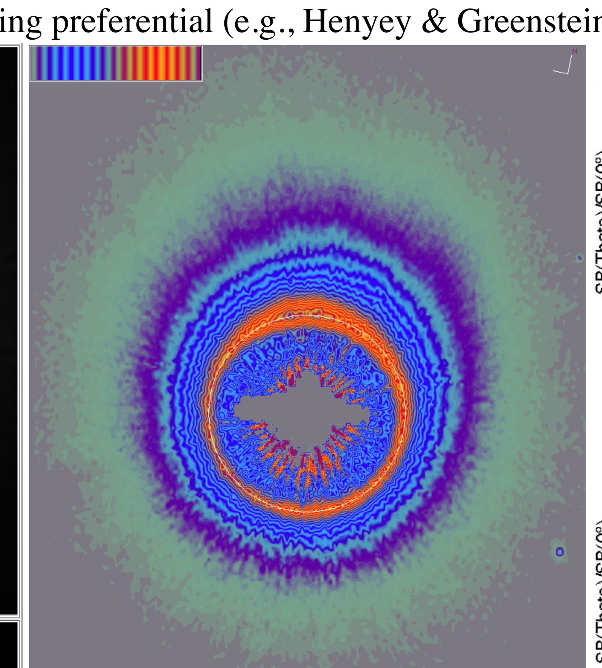

Fig 2. 0 to 6 count s^{-2} pixel^{-1} linear display. 3.125% surface brightness contours.

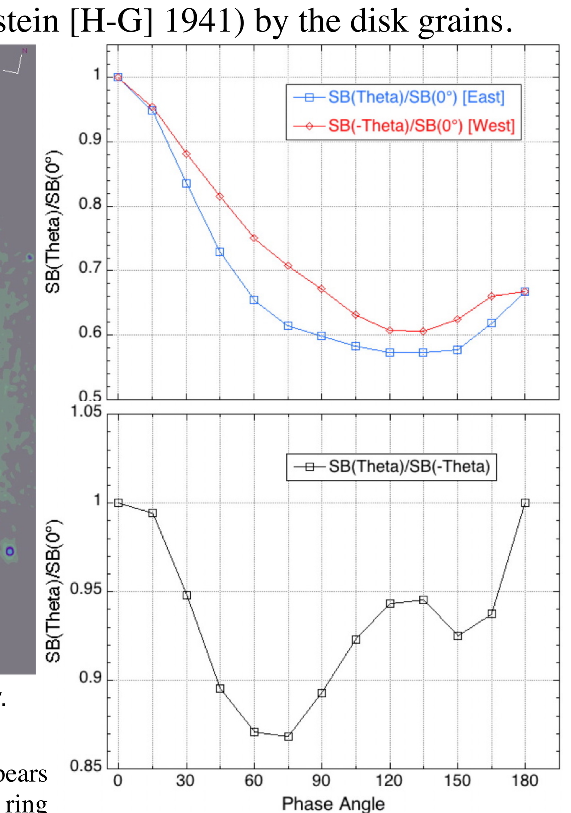

Fig 3. Azimuthal and axial non-mirror-symmetric bright-ring SB asymmetries.

Morphologically, the HD 181327 debris disk appears as an asymmetrically bright elliptical ring surrounded by a larger (and fainter) diffuse region. Assuming intrinsic circular symmetry, after elliptical isophot fitting finding a celestial PA of 102°±4° for the major axis of the bright ring inclined 30.1° ±1.2° from face-one, we "deproject" the HD 181327 disk to a face-on viewing geometry (left; with major axis horizontal). Photometric surface brightness contours external to the bright ring deviate from perfect ellipses and exhibit some azimuthal "skewing" with stellocentric distance about the presumed axially concentric bright debris ring. What is most immediately noticeable (and striking) is that: (a) the "left" and "right" sides of the debris ring, on opposite sides of the minor (vertical) axis at mirror-symmetric deprojected scattering phase angles (SCA; SCA(0°) defined here as coincident with the azimuth angle of the peak SB along the ring), are of significantly different brightness and, (b) a minimum in the surface brightness around the ring is not coincident with deprojected SCA (180)° (i.e., not H-G scattering) and also is not diametrically opposed to the direction of the "extension" of the outer disk halo to the north.

Compensating for the r^{-2} decline of the stellar radiation field with increasing stellocentric distance, we transform the SB image (below left, in face-on projected form) into a proxy for a surface density "image" of light-scattering particles (below, right) from which the sharpness of, and clearing within, the inner-edge of the bright ring is readily apparent.

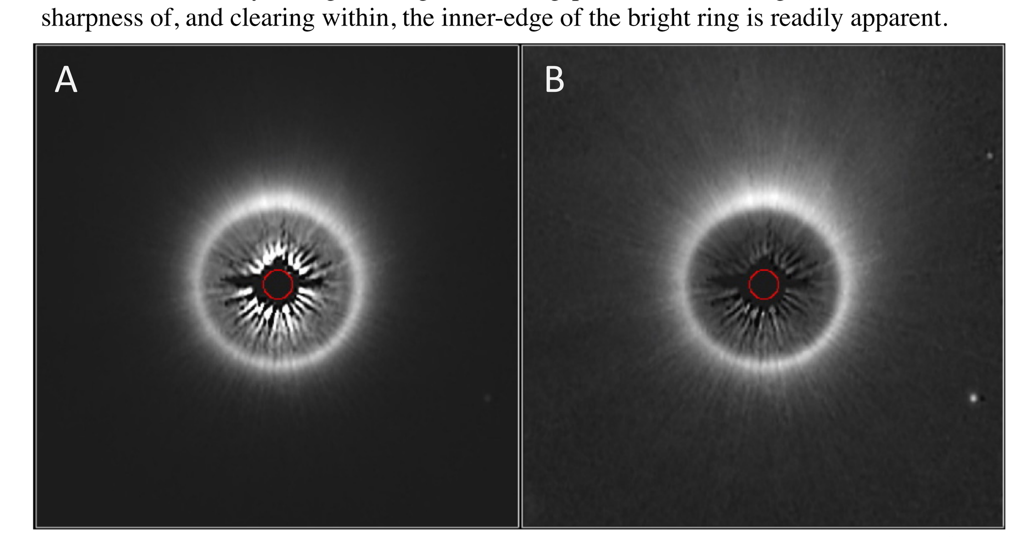

Fig 4. Face-on deprojected images before (A) & after (B) scaling by $(r/r_{ring})^2$.

Diametrically opposed radial SB profiles show mirror asymmetric behavior and asymmetries w.r.t. scattering phase angle 0°.

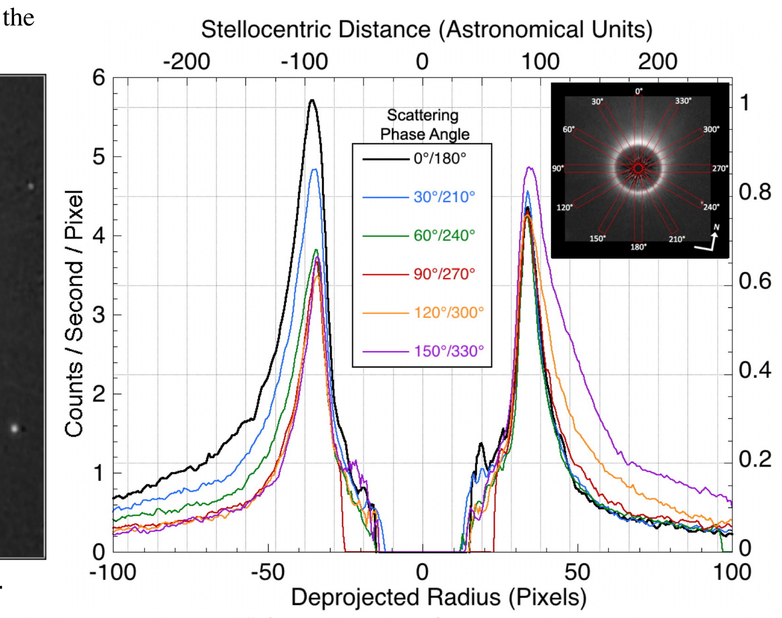

Fig 5 (above right): Stellocentric cross-sectional profiles, 10 pixels (0.507") in width, extending ± 5" from the star, from scattering phase angle 0° (where the ring central-peak is brightest) in 30° azimuthal increments (providing fully independent measures at the smallest useful inner working angles; see inset image). At scattering phase angles 180° — 270° the outer-edge profile is significantly steeper then the diametrically opposed sector, with photometric full-width to half maximum (FWHM) broadening in the latter due (perhaps) to small grains preferentially "blown" from the system toward the northeast (as also suggested directly be the distribution of low SB material at large stellocentric distance). In this 180° — 270° quadrant the FWHM of the more inner:outer symmetric bright ring is narrower than the opposite. In this quadrant we find: $FWHM_{inner\_edge}$ = 8.7 AU, $FWHM_{outer\_edge}$ = 14.7 AU (W = $FWHM_{ring}$ = 23.4 AU). With D_{ring} = 177.7 AU, W/D(180° — 270°) = 0.131.

Stellocentric offset: The location of the occulted star is accurately determined in coronagraphic images *prior* to PSF subtraction by least-squares fitting of the intersection of the (HST optical telescope assembly induced) stellar diffraction spikes (suppressed or eliminated in multi-roll combined PSF-template subtracted disk images). Separately, but using a common differential astrometric reference, the center of the debris ring apparent ellipse is determined from elliptical isophote fitting (as noted above) in disk images. Together, the two inform on any stellocentric offset of the debris ring. In the case of HD 181327 such an offset has been ascertained with respect to scattering phase angle 0° to 180° with stellocentric distances to the diametrically opposed ridge of peak radial brightness with R_ring(0°) = 93.2 ± 0.6 AU, and R_ring(180°) = 89.3 ± 0.7AU, so a 3.9 ± 0.9 AU offset (2.2% of the ring diameter), in face-on deprojection.

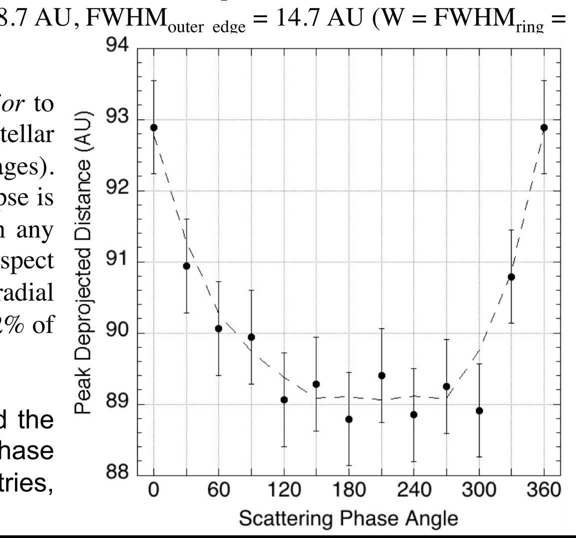

Fig 6 (right): Circumstellar measures of the radial distance to the ring peak SB every 30° around the ring are systematically consistent with the offset measured along the 0° to 180° scattering phase angles. Dynamical models invoking (unseen) planets to explain the ring profiles, disk asymmetries, and other features, must also reproduce or be constrained by this measured stellocentric offset.

AU MIC

GO/12228 "inner" disk imaging of AU Mic cleanly probe the edge-on disk mid-plane to a stellocentric distance of 5 AU. Significant out-of-plane asymmetries are seen notably on the SE side of the disk (some suggested from earlier imaging). In particular, a prominent "bump" above (to the NE) of the mid-plane at 13 AU is seen just beyond a "local minimum" in the mid-plane SB at 10 AU. Two-epoch common proper motion measures rule out background contamination.

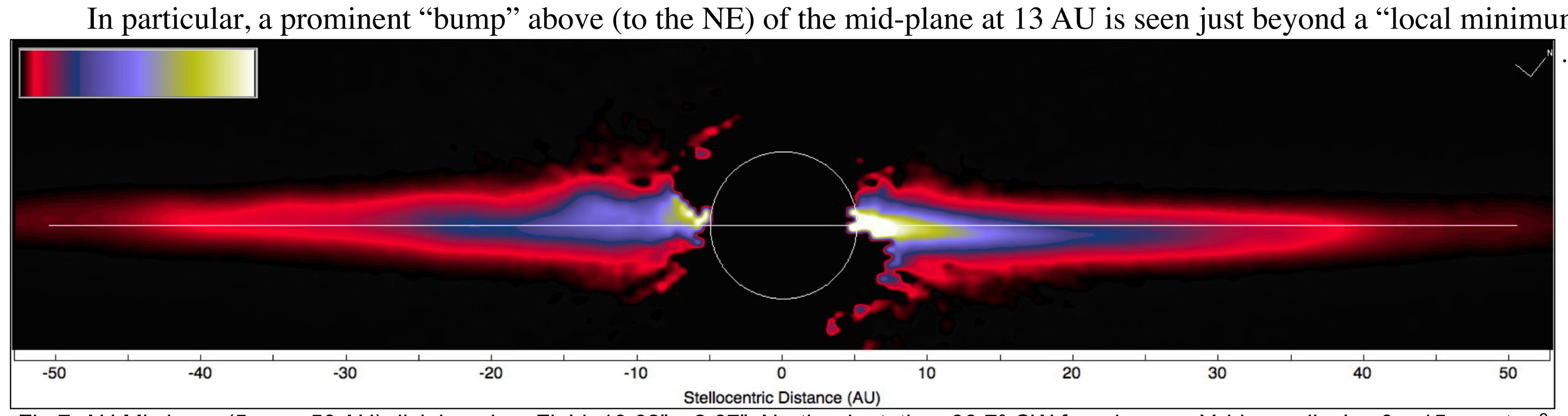

Fig 7. AU Mic inner (5 ≤ r ≤ 50 AU) disk imaging. Field: 10.62" x 2.67". North orientation: 38.7° CW from image +Y. Linear display 0 – 15 count s^{-2} pixel^{-1}. 1 count s^{-2} pixel^{-1} = 177 microJy arcsec^{-2}. White circle: 5 AU (mid-plane) inner working distance. White line is morphological disk major axis defined from 50 ≤ r ≤ 100 AU photometric isophotes (shown below).

Surface brightness isophotes (Fig 8) on the NW side of the disk at r < 50 AU "dip" below the outer (> 50 AU) disk mid-plane with increasing deviation at smaller stellocentric distances; by appx 1.5° for the innermost isophotes (< 15 AU). To further illustrate out-of-plane asymmetries, the r < 100 AU disk image below is also reproduced with a 4x expansion in vertical scale.

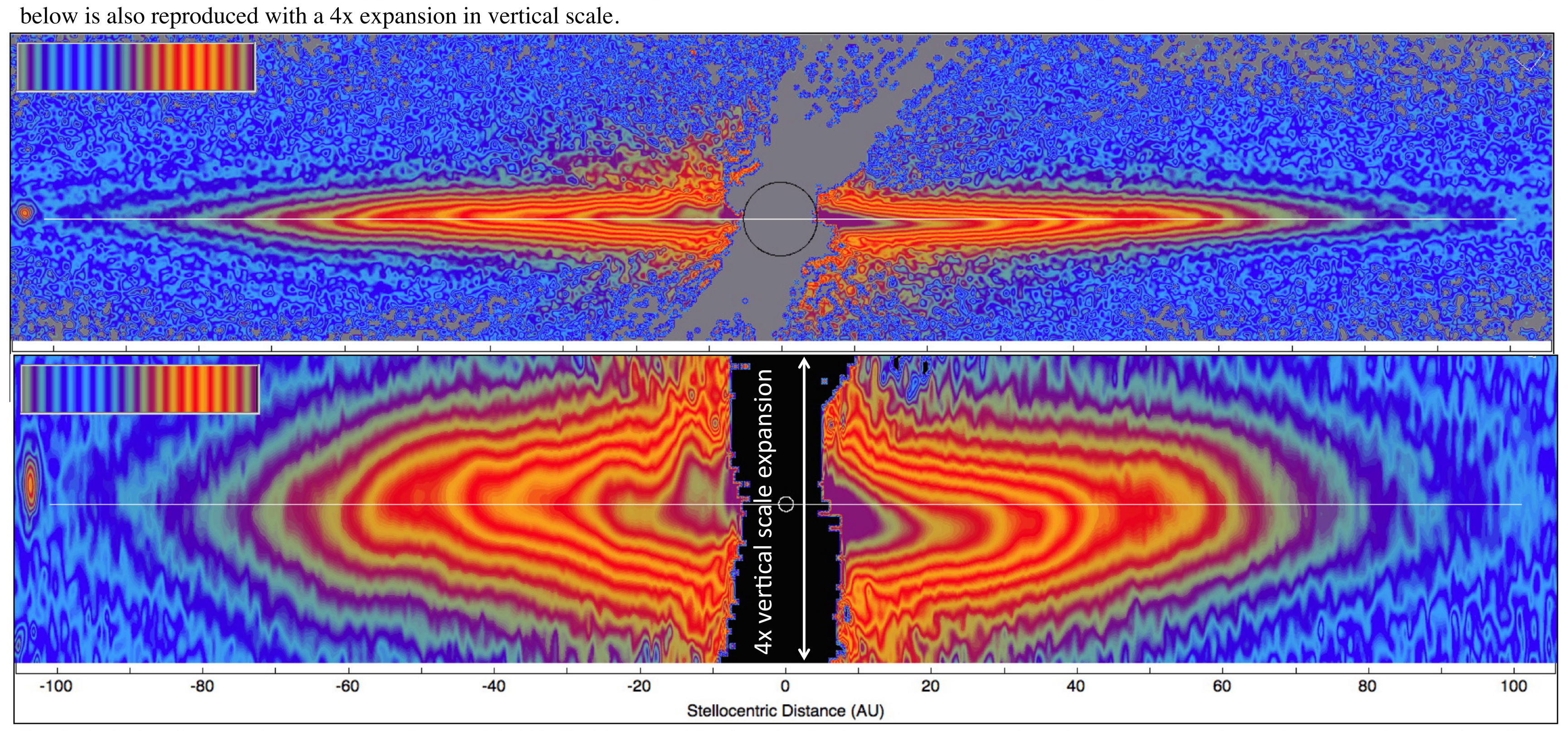

Fig 8. AU Mic disk isophote images: 5 ≤ r ≤ 50 AU. Field (top): 10.62" x 2.67", bottom 4x spatial scale expansion about disk mid-plane (white line) defined by 50 ≤ r ≤ 100 AU isophotes. North orientation: 38.7° CW from image +Y. Log10 display [3.0] to [+1.0] {dex} csp. Black circle (top): r = 5 AU mid-plane inner working distance. White line is morphological disk major axis defined from 50 – 100 AU photometric isophotes.

Fig 9 (right). Radial surface brightness profile of the AU Mic disk mid-plane, measured in a 50 mas wide central strip along the disk mid-plane defined by 50 ≤ r ≤ 100 AU photometric isophotes, ± 100 AU from the central (coronagraphically obscured) star. The 1-σ error bars are computed from the dispersion in measures from the individual PSF-subtracted images about the (up to 12-image for any single pixel) roll-combined median image and do not include likely less than few percent uncertainties in the absolute flux density calibration.

The disk surface brightness profiles on both sides of the star (Fig 9) are better fit by exponentials (green dashed lines) rather than power laws. Note the significant "break" in the NE and SW side profiles at 50 AU and other deviations elsewhere in the inner (< 50 AU) part of the disk.

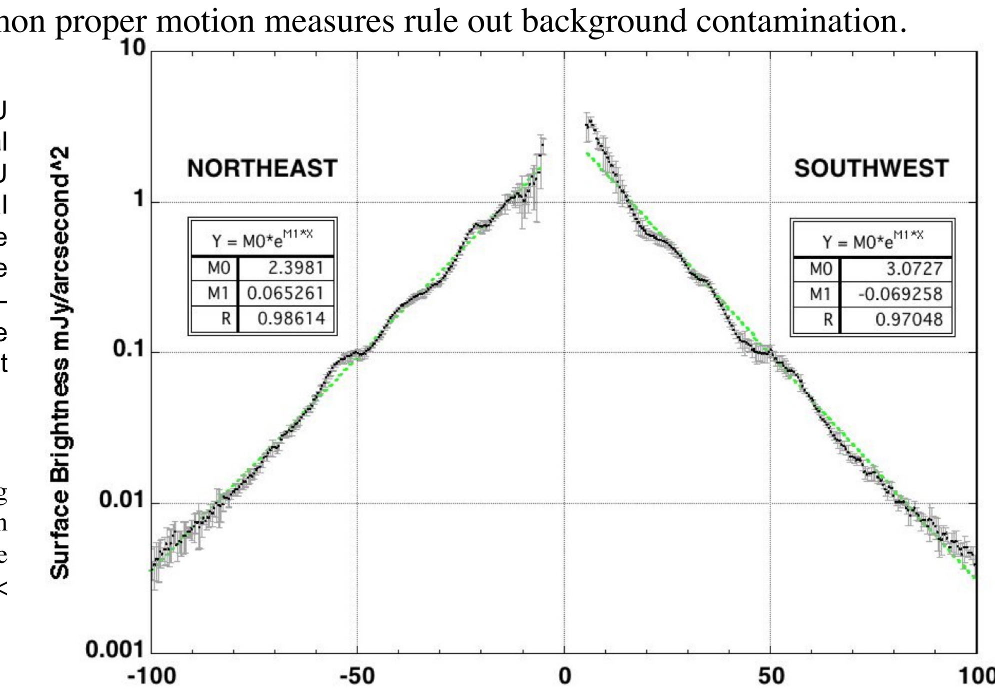

Dust-scattered starlight in the AU Mic disk (Fig 10) is detected with significance to a distance of appx 130 AU on the NE side of the disk (the "green dot" in the disk mid-plane at an apparent projected distance of 105 AU is a background star). On the SW side of the disk, light-scattering dust in the disk plane is superimposed upon a background galaxy (vermin of the sky).

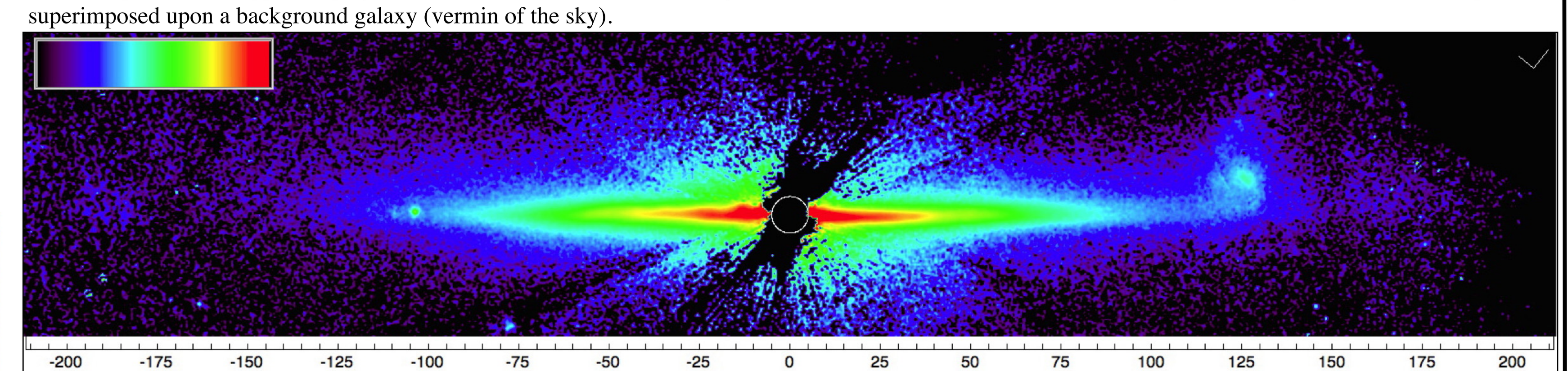

Fig 10. The full spatial extent of the AU Mic disk. FOC: 42.64" x 16.66" stretched into the dirt – log10 display from [3.0] to [+1.0] {dex} cps.

Acknowledgements: Based on observations made with the NASA/ESA Hubble Space Telescope, at the Space Telescope Science Institute (STScI), which is operated by the Association of Universities for Research in Astronomy, Inc., under NASA contract NAS 5-26555. These observations are associated with HST GO program 12228. Support for program 12228 was provided by NASA through a grant from the STScI. We acknowledge the contribuitions of the AR/11279 team in furthering our understanding, and developing mitigation strategies against, *HST* PSF instabilities, characterization, and "matching" for PSF template optimization. We thank our STScI program coordinator, Beth Perriello, for her diligent work in in optimizing the schedulability of our observing plan to maximize the science return. Part of this research was carried out at the JPL, under contract with NASA.

Contact: Dr. Glenn Schneider, Steward Observatory and the Department of Astronomy, The University of Arizona, Tucson, Arizona 85721 USA; gschneider@as.arizona.edu

HD 107146

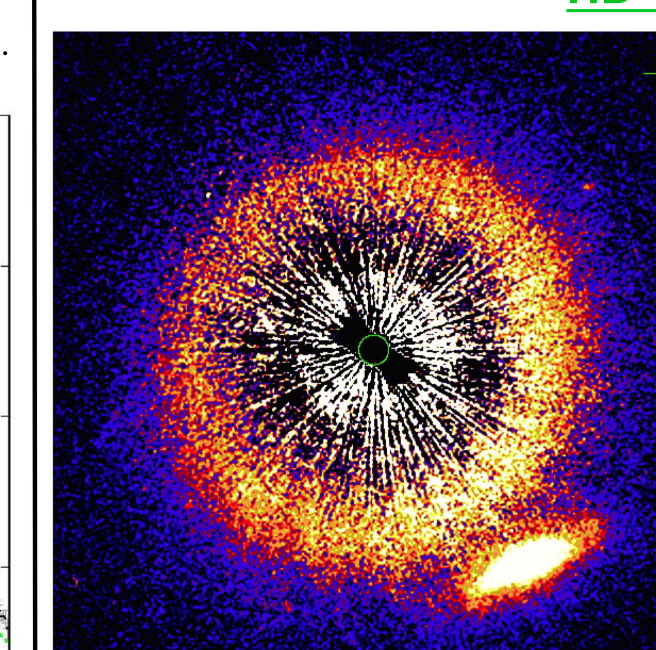

Improving on earlier ACS and NICMOS scattered-light images of HD 107146, our new STIS image sensitively traces the dust depletion in the inner regions of the broad HD 107146 debris ring to within 60 AU of the star, appx half the stellocentric distance where the debris ring is brightest.

Fig 11 (left). 15.23" x 15.23" FoV. Linear display from 0 to 8.85 μJy arcsec⁻². IWA_{eff} ≥ 0.41" pixels (r = 11.5 AU; green circle). A background galaxy pollutes the outer disk image beyond the disk minor axis to the SW (forward scattering direction).

Several point sources in close disk proximity are rejected as co-moving companions from non-common proper motion measures over two STIS epochs of observation.

Fig 12 (right). Wit a 5.5 μJy arcsec⁻² peak SB at r = 120 AU, the HD 107146 disk is > 100x fainter than the HD 181327 debris ring (see Fig 5). Dust scattered starlight steadily declines interior to the peak to near zero at a then smaller sensitivity-limited angular distances of ≤ 2".

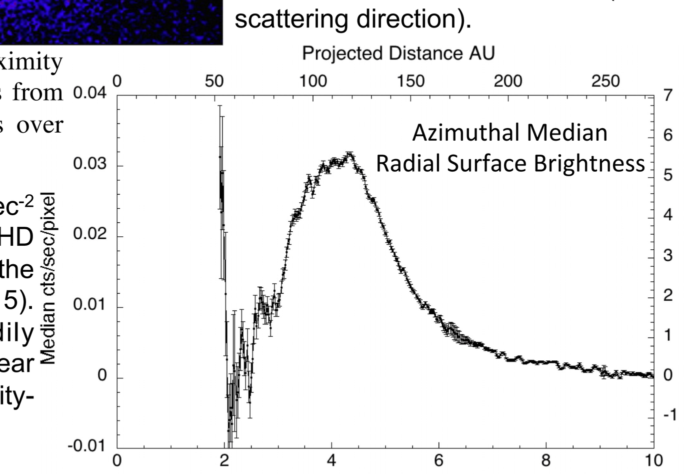

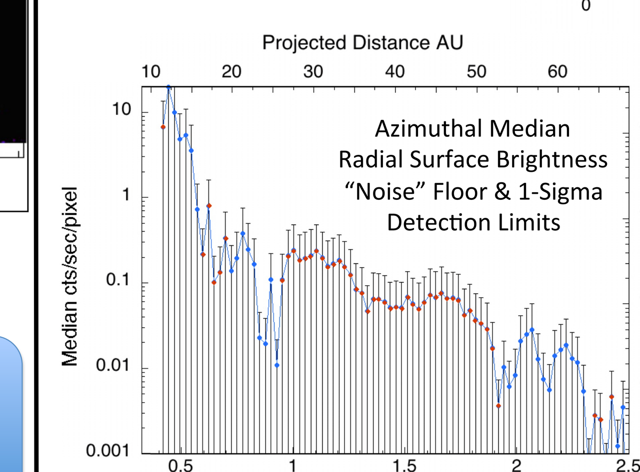

Fig 13 (left). Interior to 60 AU, to a limiting inner working distance of appx 11.5 AU, our new STIS data robustly provide dust scattered-light sensitivity limits, constraining the amount of dust that may reside interior to the dust ring.